23rd ABCM International Congress of Mechanical Engineering
December 6-11, 2015, Rio de Janeiro, RJ, Brazil

A NUMERICAL ANALYSIS OF THE EFFECTS OF SIDE WALL COMPRESSION IN 3D SCRAMJET INTAKES

Jacqueline Aparecida Reinaldo de Carvalho
Mauricio Antoniazzi Pinheiro Rosa
Divisão de Aerotermodinâmica e Hipersônica
Intituto de Estudos Avançados-IEAv
Comando Geral de Tecnologia Aeroespacial-CTA
Caixa Postal 6044
12231-970 São José do Campos-SP-Brazil
jacqueline_rcarvalho@hotmail.com*
pinheiro@ieav.cta.br**

Abstract. *This paper has the objective of studying numerically the effects of converging and non-converging scramjet intake side walls on intake airflow structures and performance. Three-dimensional (3D) calculations were performed with the CFD Fluent code to analyze the complex shock-to-shock and shock wave/boundary-layer interactions which cause vortices and flow separation at the compression ramp and side walls. A viscous flow modeling analysis was done using the turbulent Spalart-Allmaras and the transition SST models available in the code. It has been observed that the presence of side walls makes the flow very inhomogeneous at the combustor entrance and degrades somewhat the intake performance with reduction in mass capture ratio which is further accentuated by side wall compression*.

Keywords: *scramjet intake, side wall, hypersonic flow, numerical simulation*

1. INTRODUCTION

The Aerothermodynamics and Hypersonics Division (EAH) of the Institute for Advanced Studies (IEAv) is conducting a series of studies aimed at flight demonstration of a hypersonic vehicle prototype powered by an air-breathing scramjet engine (14X vehicle).

An important part of such an engine is the hypersonic air intake system whose basic requirements can be summarized as follows: be as efficient as possible by reducing energy and mass losses to a minimum, to deliver the right amount of air at the combustion chamber entrance, with tolerable flow distortion and at certain temperature and pressure, and contribute the least possible drag to the system (Mahoney, 1990)

The present work is part of a series of numerical studies for the development of suitable air intake systems for the 14-X hypersonic vehicle prototype under development at IEAv. In this context, recent numerical studies have been focused only on two-dimensional (2D) analyses of intake airflow structures and performance at nominal and off-design conditions (Moura, 2014; Moura and Rosa, 2014)). Continuing these studies, the present work purpose is to present the results of an analysis of the effects of converging and non-converging side walls on the airflow and performance (mass capture and total pressure recovery) of a 3D scramjet intake. The CFD Fluent code is used to perform the numerical calculations of the airflow with complex shock-to-shock and shock wave/boundary-layer interactions (SWBLI), which cause vortices and flow separations at the compression ramp and side walls of the intake. Of special interest is the airflow conditions at the interface between intake and combustor, i.e., the intake exit plane, which showed to be very inhomogeneous, however the developing corner vortices produce a region of high temperature that can ensure self-ignition for low temperature experimental test runs (Reinartz, 2009, Krause and Ballmann, 2007).

2. Numerical methods and models

The software ANSYS Fluent version 15.0 was used to analyze numerically the hypersonic airflow in a 3D scramjet intake. The viscous models employed in this analysis are all based on the filtered compressible Reynolds-Averaged Navier-Stokes (RANS) set of conservation equations. Considering the air as a calorically perfect gas and using some additional closing relations:

$$\frac{\partial \rho}{\partial t} + \nabla \cdot (\rho \vec{v}) = 0 \tag{1}$$

$$\frac{\partial}{\partial t}(\rho \vec{v}) + \nabla \cdot (\rho \vec{v}\vec{v}) = -\nabla p + \nabla \cdot \left(\bar{\bar{\tau}}_{eff}\right) \tag{2}$$

$$\frac{\partial}{\partial t}(\rho E) + \nabla \cdot [\vec{v}(\rho E + p)] = \nabla \cdot \left[k_{eff} \nabla T + \left(\bar{\bar{\tau}}_{eff} \cdot \vec{v}\right)\right] + S_h \quad (3)$$

$$E = h - \frac{P}{\rho} + \frac{v^2}{2} \quad (4)$$

$$dh = c_p \, dT \quad (5)$$

$$p = \rho R T \quad (6)$$

where ρ is the density, $\vec{v}$ is the velocity vector, p is the pressure, E is the total energy, T is the temperature, h is the enthalpy, c_p is the specific heat at constant pressure and R is the gas constant. The effective viscous stress tensor, $\bar{\bar{\tau}}_{eff}$ is given by Eq. 7.

$$\bar{\bar{\tau}}_{eff} = \mu_{eff} \left[(\nabla . \vec{v} + \nabla . \vec{v}^T) - \frac{2}{3} \nabla \ . \ \vec{v} I\right] \quad (7)$$

where I is the unit tensor and μ_{eff} is the effective viscosity. The second term on the right-hand side represents the effect of volume dilation. The subscript *eff* in Eq 3 means the effective values, which adds the turbulent term whenever a turbulent model is in use, i.e, $k_{eff} = k_t$ + k.

The simulations have been performed with the finite volume density-based solver available in ANSYS Fluent, which solves Eq. 1 to 3 as a coupled set, followed by additional scalars, such as equations for the turbulence models, which are solved independently.

The viscous flow models used in this analysis are the turbulent Spalart-Allmaras (SA) and the Transition SST, which will be briefly explained here. The first one solves a modelled transport equation for the kinematic eddy viscosity and was developed for aerospace applications with wall-bounded flows (Spalart and Allmaras, 1992). And the second one, the Transition SST model is a modification of the SST k-ω, just coupling it with two more transport equations, one for intermittency and another for the transition onset criteria (Menter et al., 2006).

2.2 Geometry and mesh

The 3D intake geometry used in the following analysis was the one used by *Reinartz, 2009.* Figure 1 shows different views of this intake. As seen, the intake has only one compression ramp with $15.5^{\underline{0}}$ angle followed by a straight duct representing a short isolator. The sweep angle of the side walls is $35^{\underline{0}}$ and compression, given by the δ_{sw} angle, extends from the side wall leading edge to the y-z plane passing through the cowl tip. As can be seen in this figure, the intake geometry presents a x-y symmetry plane at half width of the isolator so that the computational domain can be reduced by a half.

At the inflow boundary, a Mach 8, T = 206 K, p = 1126 Pa incoming horizontal free stream is considered for the analysis. For the supersonic outflow, the variables are extrapolated from the interior. At solid walls, the no-slip condition is enforced by setting the velocity components. Uniform constant temperature at the walls of 293 K is considered. Figures 2 and 3 show the structured meshes at the symmetry plane and the intake exit plane, respectively. The two details show the critical nose region and the area where flow expansion occurs at the isolator entrance. For the half model computation domainthe grid size is about 4.5 million points: 360 in the streamwise direction and 103 x 122 in the cross plane. The grid spacing is condensed near the walls and the leading edges of ramp and cowl, otherwise, is quite homogeneous

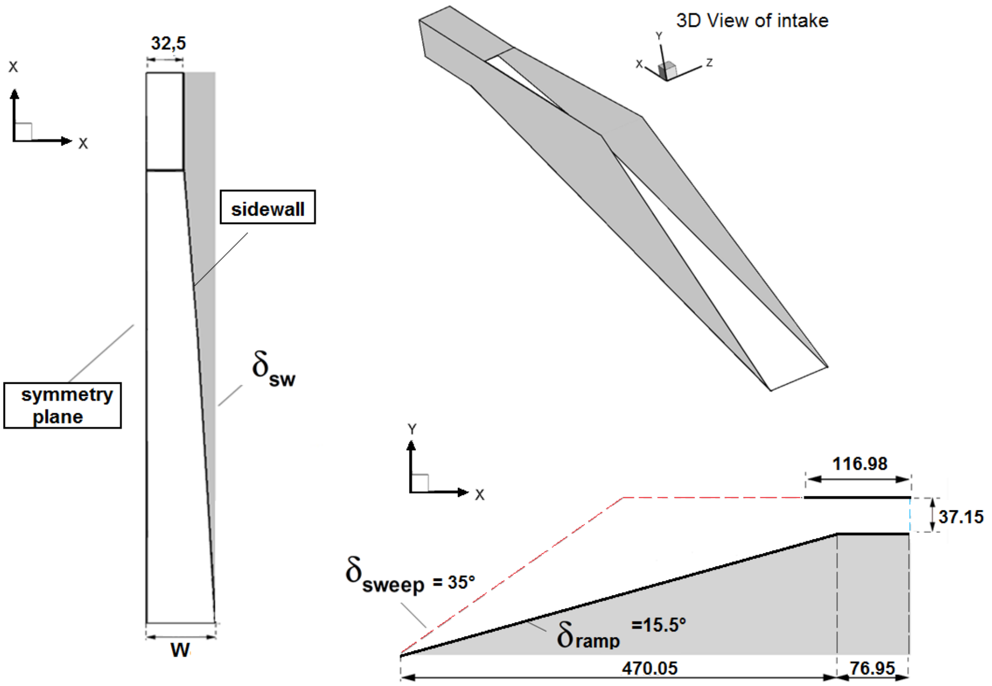

Figure 1- Intake geometry with side wall compression used in the analysis (Reinartz, 2009)

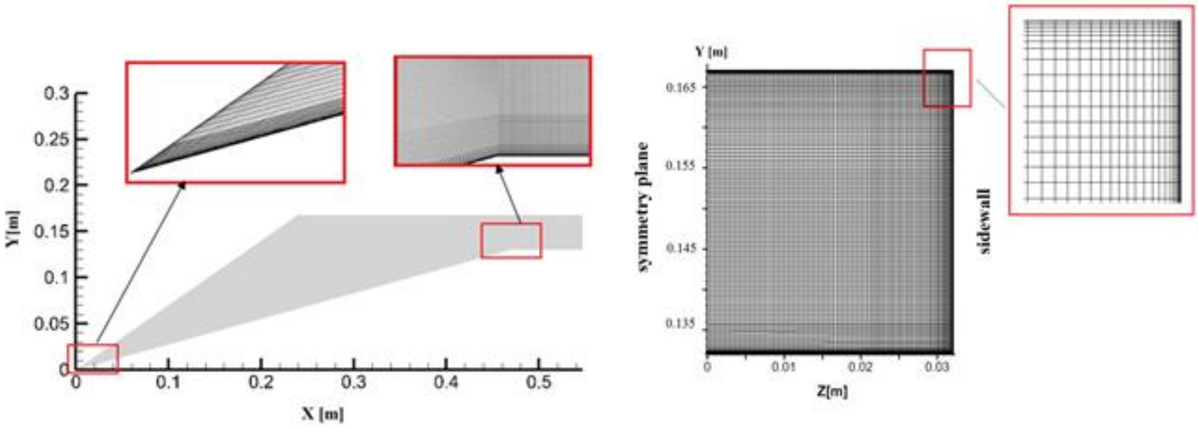

Figure 2- Grid cell distribution at symmetry plane and exit plane for the 3D intake

3. Results

In the following analysis, two cases are considered regarding the side wall compression angle: $\delta_{sw} = 0^{\underline{0}}$ (non-converging) and $\delta_{sw} = 3.5^{\underline{0}}$ (converging) side walls.

Figure 3 shows the Mach number contours on the symmetry plane for $\delta_{sw} = 3.5^{\underline{0}}$ compression side walls using the Spalart-Allmaras (SA) model. Also sketched in this figure are the shock waves for inviscid flow for converging and non-converging side walls. For inviscid flow and non-converging side walls, the ramp shock wave basically passes through the cowl tip since the shock-on-lip condition has been used for the intake design. For the case with converging side walls, it can be seen that the shock wave is that given by the ramp up to about 0.23 meter from the leading edge and then bends outwards due to its interaction with the side wall shock wave. This produces a gap between the shock wave and the cowl tip which causes flow spillage. As can be seen in Fig. 3, viscous effects accentuate even more flow spillage, which can be also confirmed by the MCR (mass capture ratio) results in Table 1.

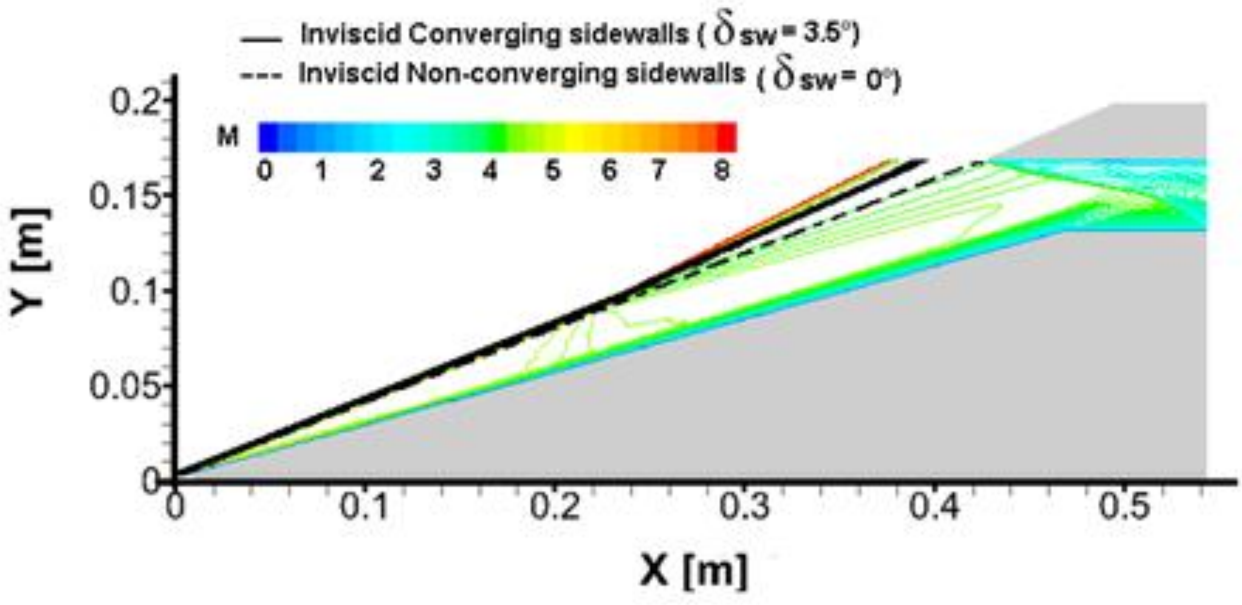

Figure 3- Mach contours on the symmetry plane for 3.5 degree converging side walls with the SA model.

Two viscous flow models have been used in the analysis, the turbulent Spalart-Alamaras (SA) and the transition SST models available in the Fluent code. The effect of compression side walls is clearly seen in Figure 4 by comparing the pressure coefficient on the ramp and cowl at the symmetry plane, for non-converging and converging side walls. For the latter, it can be seen that the effect of the compression side wall shock wave on the ramp pressure is to increase it with consequent increase of pressure on the cowl too. Comparing the pressure coefficient for both viscous models in Figure 4, it is noticed that they are actually close to each other. However, as seen in Table 1, the transitional SST model presents slightly better performance results than the turbulent SA model probably because it generates thinner boundary-layer. The results in Fig. 3 and 4 are similar to the ones presented by *Reinartz, 2009* (Fig. 7).

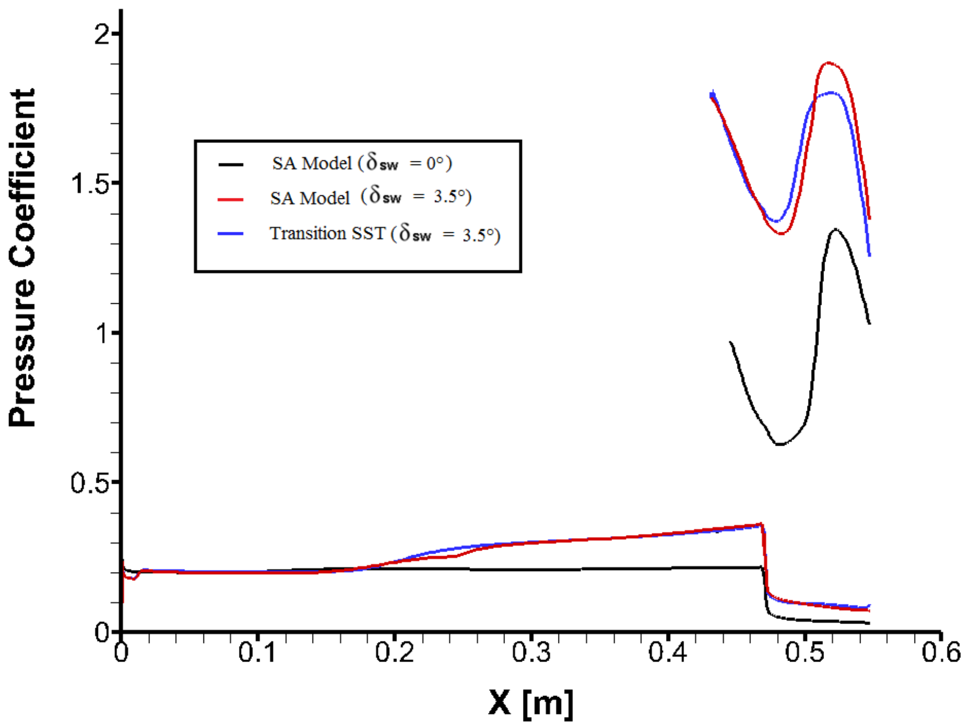

Figure 4-Ramp and cowl pressure coefficient distributions at the symmetry plane for different viscous models.

Figure 5 and 6 show Mach number contours at several planes and views for 3.5 degree compression walls for inviscid and viscous flow with the transition SST model, respectively. The inviscid flow results show the shock waves, and their interactions, generated in the 3D intake geometry with compression side walls which is helpful for comparison to observe more clearly the viscous effects on the intake flow structure. The additional Mach contours at some vertical planes in the ramp domain show the resulting shock structure from the converging side wall and the ramp shock wave interactions. It can be seen that the side wall shock wave plane is somewhat inclined with respect to the ramp because of the sidewall sweep angle (see Fig. 1). The Mach number contour at the horizontal plane shows the 3.5 degree side wall oblique shock wave and its interaction with the ramp shock wave. Also shown in this figure is the flow inside the isolator with the presence of the cowl reflected shock wave. As can be seen in Fig. 6, which shows the Mach number contour for viscous flow, vortices are generated in the corner between the ramp and the side walls yielding zones where the slow and hot boundary layer material is transported away and other regions where the boundary layer is thickened, leading to flow separation zones on the sidewalls and on the ramp. These additional separations generate additional shock - shock interactions yielding very complex flow structures near the walls. All these effects have a huge impact on the intake flow and result in loss of intake performance as they reduce both mass capture and total pressure recovery, as shown in Table 1.

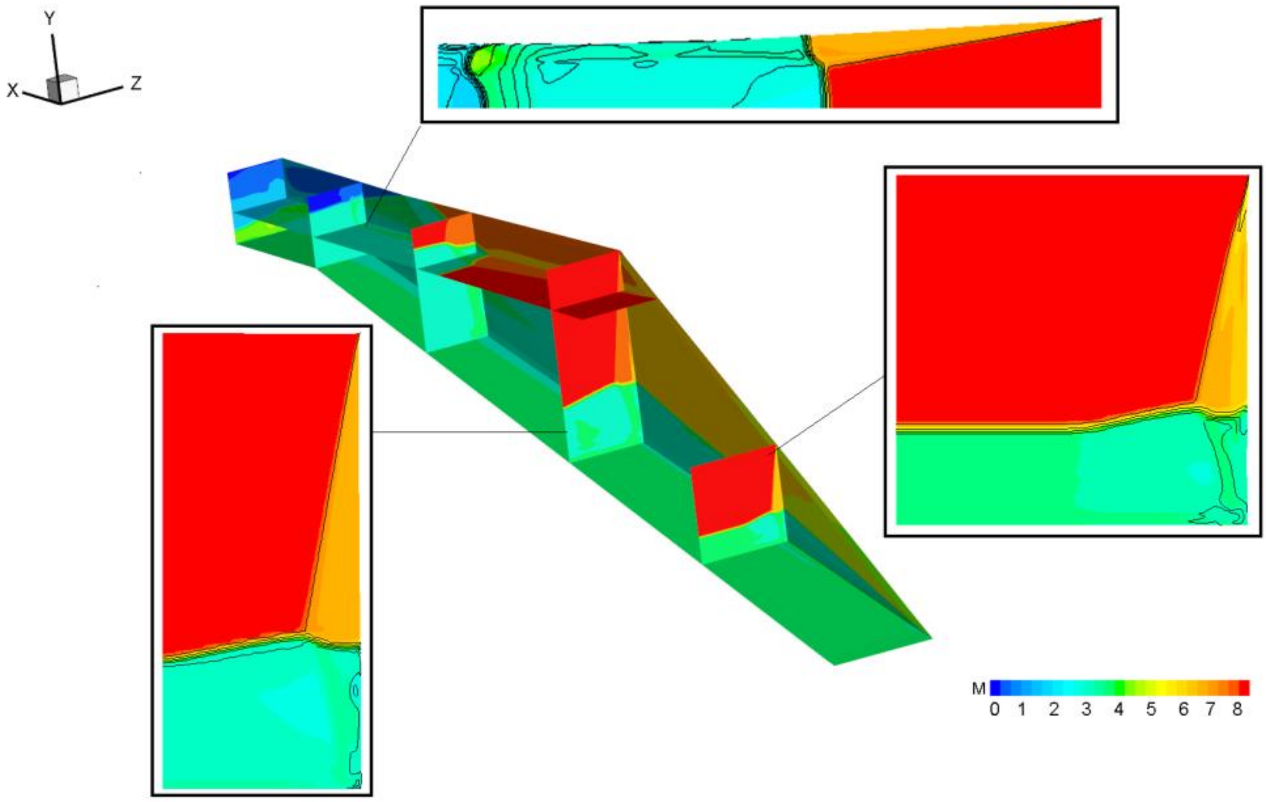

Figure 5-Mach number contours for inviscid flow for the 3.5 degree converging side wall intake.

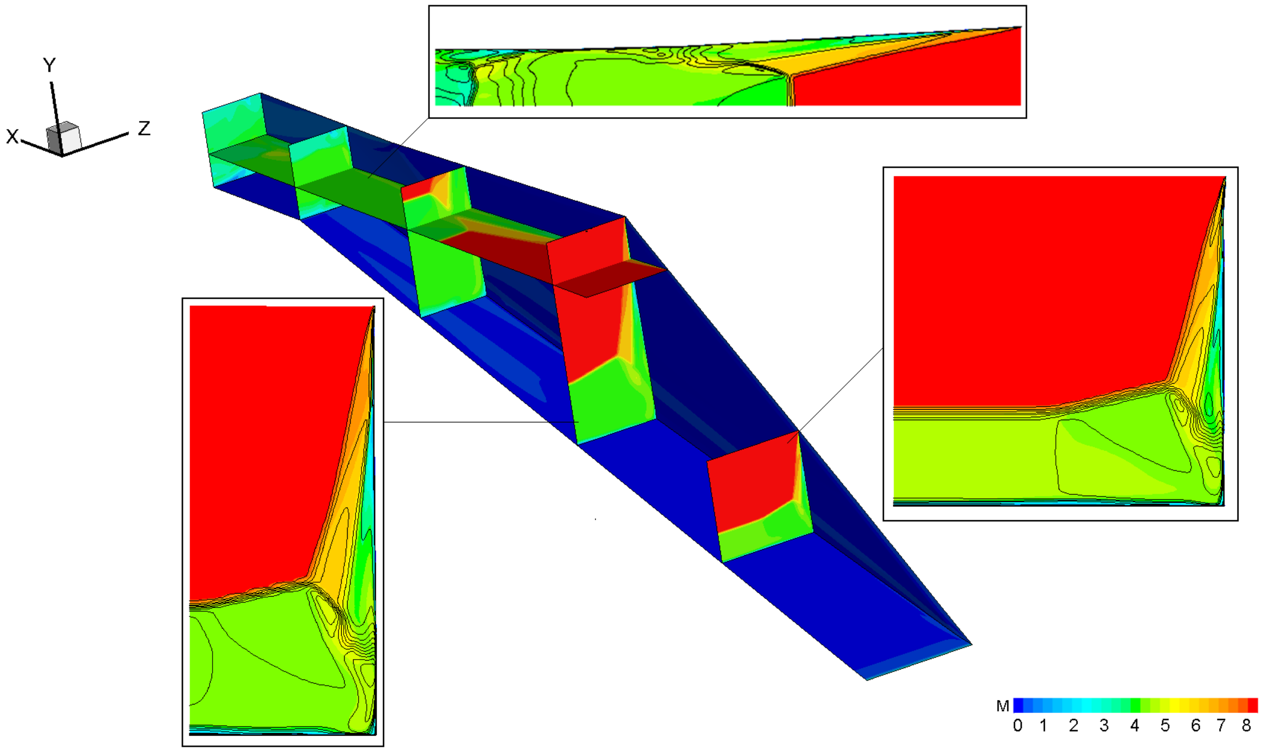

Figure 6- Mach number contours for viscous flow with the Transition SST model for the 3.5 degree converging side wall intake.

Figure 7 and 8 show the numerically calculated Mach number contours at the intake exit plane for non-converging and converging side walls, respectively, for inviscid and viscous flow models. As can be seen in Fig. 7, although there is no flow compression due to side wall angle, the flow structure on the exit plane is considerably affected by viscous modeling when compared with the inviscid results. This has to do basically with flow separation on the side walls caused by the ramp shock wave. It can be noticed in Table 1 that the performance parameters (mass capture and total pressure recovery) are quite affected by the side walls, when they are compared with the respective 2D results, reducing considerably the intake performance. The results in both figures show that the presence of side walls makes the flow at the exit plane very inhomogeneous, no matter if they are converging or non-converging. Figure 9 shows the temperature distributions at the exit plane for both converging and non-converging side walls. Due to the flow inhomogeneity, regions of high and low temperatures are present, which produce high thermal loads to the structure. Both cases have a hot region at the corner between the ramp and the side wall and at the top of the isolator, although, the converging side wall case, besides to show higher temperatures, also presents a larger hot region which extends from the top to the middle of the isolator.

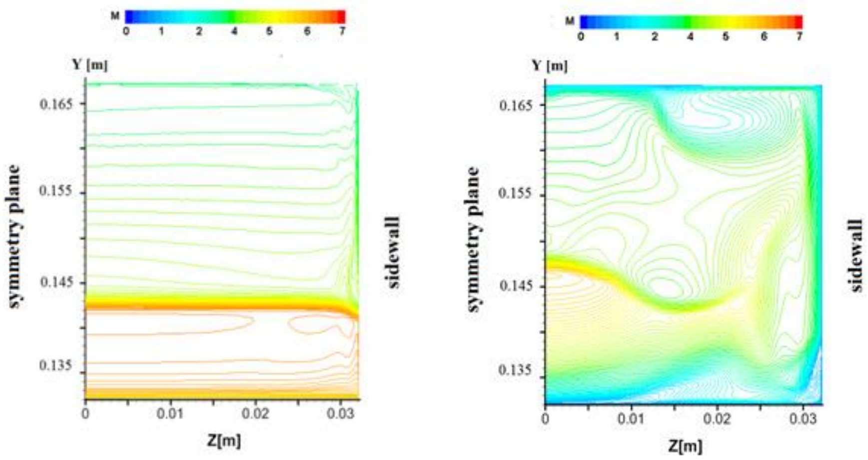

Figure 7-Mach number contours at exit plane for the non-converging side wall intake: inviscid flow (left); viscous flow with the transition SST model (right).

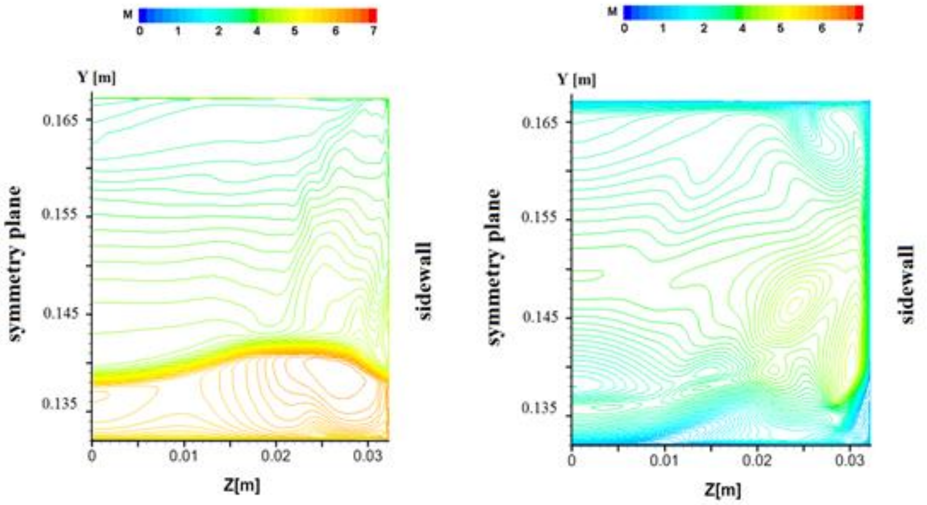

Figure 8- Mach contours at exit plane for the 3.5 degree converging side wall intake: inviscid flow (left); viscous flow with the transition SST model (right).

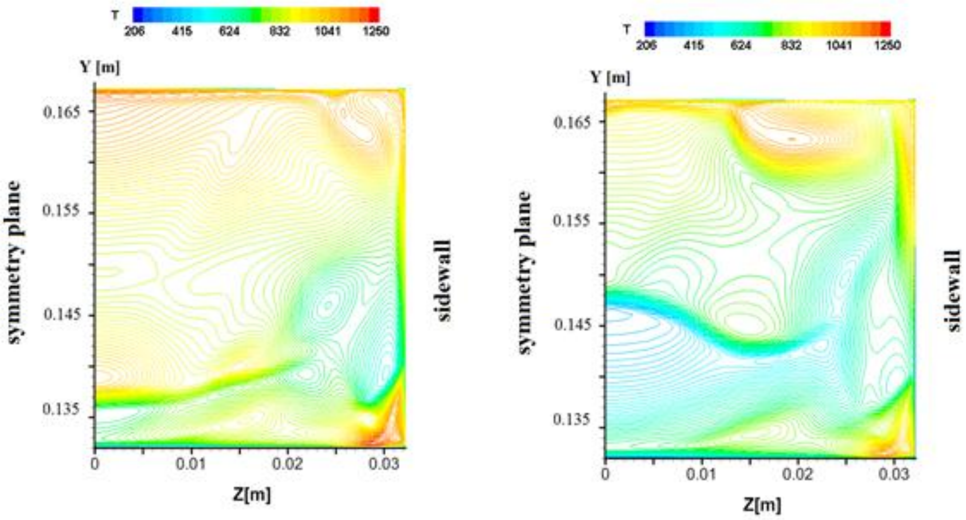

Figure 9-Temperature distributions at the exit plane: converging side walls (left); non-converging sidewalls (right).

It can be observed in Table 1, which presents some intake performance parameters and also average flow properties at the intake exit plane for 3D geometries with converging and non-converging side walls and also for 2D planar geometry, that, although the mass capture ratio (MCR) gets smaller for increasing converging side wall angles, the mass flow rate into the intake gets higher because of the higher available mass flow rate for converging side walls. Also can be seen in this table that both viscous and side wall compression effects are to increase the average pressure and temperature and reduce Mach number at the combustor entrance.

4. CONCLUSIONS

This work presented the results of a preliminary analysis of 3D intakes with focus on the effects of converging and non-converging side walls on the intake airflow structure and performance (mass capture and total pressure recovery).

The numerical calculations have shown that the airflow in the analyzed intake presented very complex flow structure with the presence of vortices and flow separations for both converging and non-converging side walls. Also, side walls have the effect of increasing flow spillage, degrading slightly the intake performance and yielding very inhomogeneous flow at the combustor entrance. On the other hand, compression side walls shorten the intake and produce hot spots at the isolator exit which may be important for experiments in shock tunnels and for combustion studies.

The 3D intake numerical analyses should continue by focusing now on the study of intakes for the 14X hypersonic vehicle prototype.

Table 1-Intake performance parameters and average flow properties at the intake exit plane

Computacional Geogmetry	**Viscous model**	**Sidewall Angle**	MCR	PR	Mass capture (kg/s)	P (kPa)	T (K)	Mach number
2D	Inviscid	-----	0.989	0.243	0.453	21.7	645	4.44
	SA	-----	0.941	0.155	0.431	22.3	758	3.50
	SST	-----	0.964	0.185	0.442	21.8	692	3.87
3D	Inviscid	0	0.989	0.243	0.453	21.7	645	4.44
	SA		0.854	0.134	0.406	21.0	766	3.40
	SST		0.880	0.157	0.420	21.0	742	3.53
	Inviscid	2	0.885	0.248	0.562	25.0	713	4.14
	SA		0.800	0.141	0.508	28.5	849	3.18
	SST		0.827	0.154	0.525	29.0	824	3,24
	Inviscid	3.5	0.841	0.352	0.634	32.5	735	4.05
	SA		0.780	0.149	0.588	34.8	900	3.07
	SST		0.804	0.162	0.606	35.3	873	3.12

5. ACKNOWLEDGEMENTS

The authors would like to acknowledge CNPq for the financial support provided to project number 560143/2010-9.

6. REFERENCES

Ansys, Fluent 15.0 User’s Guide, 2014.

Mahoney, J.J., 1990. Inlets for Supersonic Missiles. AIAA Education Series, Washington, DC, 1st edition.

Krause and Ballmann, 2007, *Numerical Simulations and Design of a Scramjet Intake Using Two Different RANS Solvers,* AIAA Conference, AIAA 2007 -5423, Cincinnati, OH, USA.

Menter, F.R., Langtry, R.B., Likki, S.R., Suzen, Y.B., Huang, P.G. and Volker, S., 2006. “A Correlation-Based Transition Model Using Local Variables—Part I: Model Formulation”. Journal of Turbomachinery, Vol. 128, No. 3, p. 413. ISSN 0889504X. doi:10.1115/1.2184352. URL http://turbomachinery.asmedigitalcollection.asme.org/article.aspx?articleid=1467239 .

Moura, A.F., 2014. A computational study of the airflow in scramjet intakes. Master’s thesis, Instituto Tecnológico de Aeronáutica, São José dos Campos, Brazil.

Moura, A.F., Rosa, M. A. P. 2014, *A numerical Investigation of scramjet engine air intakes for the 14-X hypersonic vehicle*.In *6 th European Conference on Computational Fluid Dynamics*, ECFD VI, 2014, Barcelona, Spain.

Reinartz, B., Behr, M., 2009, “*Influence of Sidewall Compression on Hypersonic Intake Performance*”, AIAA Paper 2009-7351.

7. RESPONSIBILITY NOTICE

The authors are the only responsible for the printed material included in this paper.